ARTICLE

Heterozygous *IDH1*$^{R132H/WT}$ created by "single base editing" inhibits human astroglial cell growth by downregulating YAP

Shuang Wei[1,2,3] · Jie Wang[4] · Olutobi Oyinlade[2,5] · Ding Ma[2,3] · Shuyan Wang[2,3] · Lisa Kratz[2] · Bachchu Lal[2,3] · Qingfu Xu[2,3] · Senquan Liu[6] · Sagar R. Shah[7,8] · Hao Zhang[9] · Yunqing Li[2,3] · Alfredo Quiñones-Hinojosa[7] · Heng Zhu[5,10] · Zhi-yong Huang[11] · Linzhao Cheng[6] · Jiang Qian[4] · Shuli Xia[2,3]

Abstract
Mutations in the isocitrate dehydrogenase 1 (*IDH1*) gene have been identified in a number of cancer types, including brain cancer. The Cancer Genome Atlas project has revealed that *IDH1* mutations occur in 70–80% of grade II and grade III gliomas. Until recently, most of the functional studies of *IDH1* mutations in cellular models have been conducted in overexpression systems with the IDH1 wild type background. In this study, we employed a modified CRISPR/Cas9 genome editing technique called "single base editing", and efficiently introduced heterozygous IDH1 R132H mutation (*IDH1*$^{R132H/WT}$) in human astroglial cells. Global DNA methylation profiling revealed hypermethylation as well as hypomethylation induced by *IDH1*$^{R132H/WT}$. Global gene expression analysis identified molecular targets and pathways altered by *IDH1*$^{R132H/WT}$, including cell proliferation, extracellular matrix (ECM), and cell migration. Our phenotype analysis indicated that compared with IDH1 wild type cells, *IDH1*$^{R132H/WT}$ promoted cell migration by upregulating integrin β4 (ITGB4); and significantly inhibited cell proliferation. Using our mutated *IDH1* models generated by "single base editing", we identified novel molecular targets of *IDH1*$^{R132H/WT}$, namely Yes-associated protein (YAP) and its downstream signaling pathway Notch, to mediate the cell growth-inhibiting effect of *IDH1*$^{R132H/WT}$. In summary, the "single base editing" strategy has successfully created heterozygous *IDH1* R132H mutation that recapitulates the naturally occurring IDH1 mutation. Our isogenic cellular systems that differ in a single nucleotide in one allele of the *IDH1* gene provide a valuable model for novel discoveries of *IDH1*$^{R132H/WT}$-driven biological events.

Introduction

In 2008, The Cancer Genome Atlas (TCGA) unexpectedly identified a mutation in the isocitrate dehydrogenase 1 (*IDH1*) gene in human glioblastoma (GBM) tumor samples

✉ Shuli Xia
  xia@kennedykrieger.org

1 Department of Respiratory and Critical Care Medicine, Tongji Hospital, Tongji Medical College Huazhong University of Science and Technology, 430030 Wuhan, China

2 Hugo W. Moser Research Institute at Kennedy Krieger, Baltimore, MD 21205, USA

3 Department of Neurology, Johns Hopkins School of Medicine, Baltimore, MD 21205, USA

4 Department of Wilmer Eye Institute, Johns Hopkins School of Medicine, Baltimore, MD 21205, USA

5 Department of Pharmacology and Molecular Sciences, Johns Hopkins School of Medicine, Baltimore, MD 21205, USA

6 Department of Medicine, Johns Hopkins School of Medicine, Baltimore, MD 21205, USA

7 Department of Neurologic Surgery, Mayo Clinic, Jacksonville, FL 32224, USA

8 Department of Biomedical Engineering, Johns Hopkins School of Medicine, Baltimore, MD 21205, USA

9 Department of Molecular Microbiology and Immunology, Bloomberg School of Public Health, Baltimore, MD 21205, USA

10 Center for High Throughput Biology, Johns Hopkins School of Medicine, Baltimore, MD 21205, USA

11 Department of General Surgery, Tongji Hospital, Huazhong University of Science and Technology, 430030 Wuhan, China

[1]. Subsequent analysis revealed that *IDH1* mutations occur in 70–80% of grade II and grade III astrocytoma and oligodendroglioma (by the legacy WHO 2007 criteria) [2, 3], as well as in other non-CNS malignancies including acute myeloid leukemia[4], cholangiocarcinomas, melanomas, and chondrosarcomas [5]. In 2016, the WHO classification of brain tumors uses IDH1 mutation as one of the molecular parameters in addition to histology to define many tumor entities [6].

Extensive genomic profiling studies identified that 90% of *IDH1* mutations harbor a heterozygous point mutation with a single base substitution of guanine (G) to adenosine (A), thus arginine (R) to histidine (H) substitution at codon site 132 (R132H). Moreover, mutations of the *IDH1* gene have been identified as one of the earliest events in glioma development [7]. Other genetic mutations tend to co-exist with *IDH1* mutations. For example, 80% of astrocytomas with *IDH1* mutations harbor *TP53* mutations and/or *ATRX* mutations [2, 7]; while *IDH1*-mutated oligodendrogliomas frequently have co-deletions of chromosome 1p and 19q [8].

Intriguingly, even though *IDH1* mutations have been identified in many cancers, and are believed to contribute to tumorigenesis, clinical studies have revealed that brain tumor patients with mutated *IDH1* survive longer and respond better to therapies than those harboring *IDH1* wild type, Thus, it is critical to dissect the biological functions of *IDH1* mutations, and to determine the molecular basis of their function during tumor initiation and tumor response to therapies. Numerous studies have investigated the biological function of mutated *IDH1*, however, the exact mechanisms by which mutated *IDH1* drives oncogenesis and facilitates better prognosis are still not fully understood, partially due to the scarcity of cellular model systems for in vitro and pre-clinical in vivo studies. It has been reported that establishing sustainable cell lines harboring *IDH1* mutations was difficult [9]. Most IDH1 functional studies have been conducted by overexpressing mutant IDH1 in cells with the IDH1 wild type background; only a few models have been established with endogenous *IDH1* mutations, most of them orthotropic xenografts [10]. These overexpression systems have played important roles in identifying the metabolite, epigenetic modulation and gene regulation of mutated *IDH1*, and have shed light on the possible molecular mechanisms of *IDH1* mutation-driven biological events. However, in the overexpression systems, the actuate regulation of the mutant IDH1 enzyme does not reflect what happens in real tumor cells. In addition, naturally occurring *IDH1* mutations may trigger metabolic stress in cells, which cannot be captured with the overexpression systems. Thus, establishing clinically relevant cellular models with monoallelic *IDH1* mutations is desired to recapitulate the biological functions of this important gene, and to dissect the molecular events involved in

tumorigenesis and tumor response to therapies driven by mutated *IDH1*.

The CRISPR/Cas9-based genome editing technique provides a powerful tool to manipulate genome structure, and opens up new opportunities for detailed studies of oncogenes and tumor suppressors [11]. CRISPR/Cas9 methods are frequently used to generate insertion/ deletion or frame-shift in a given genome via non-homogenous end joining with high efficiency. However, generating site-specific mutations or programmed editing by CRISPR/Cas9 depends on homologous recombination, which happens at a very low rate [12]. Recently, Komor et al. [13] created a chimeric enzyme consisting of a catalytically dead Cas9 (dCas9) and a cytidine deaminase that is able to introduce a C to T point mutation with very high efficiency (~70%) (or G to A in the complementary strand). In this study, we took advantage of the new "single base editing" technique and successfully generated heterozygous *IDH1* R132H mutation (*IDH1^{R132H/WT}*) in human astroglial cells with high efficiency (~20%). We utilized these isogenic cellular systems that differ in a single nucleotide in one allele of the *IDH1* gene, and determined the epigenetic alteration, gene expression, phenotype, and signaling transduction pathways driven by heterozygous *IDH1^{R132H/WT}* in human astroglial cells.

Results

Generating heterozygous *IDH1* R132H mutation (*IDH1^{R132H/WT}*) in human astroglial cells

Human astroglial cell line SVG was originally established from human fetal brain tissues and immortalized with an origin-defective mutant of simian virus 40 (SV40) [14]. A subclone of SVG, SVG-10B1 [15], was used as a model system to study the biological function of *IDH1^{R132H/WT}*. In order to generate a point mutation, that is CGT (R) to CAT (H), at the exon 4 of the *IDH1* gene in one allele of the genome, we adopted a state-of-the-art and highly efficient "single base editing" technique developed by Komor et al. [13], which employs a fusion enzyme of catalytically dCas9 and cytidine deaminase to introduce a C to T point mutation. IDH1 guide RNA (gRNA) was designed to have the edited site "C" within the activity window of cytidine deaminase to change the code G to A in the complementary strand (Fig. 1a). The precise cut of the *IDH1* gene was validated by co-transfecting HEK293 cells with wild type Cas9 and the *IDH1* gRNA followed by T7E1 digestion (Supplemental Fig. 1a, b). SVG cells were transfected with the *IDH1* gRNA and the fusion enzyme, followed by antibiotic selection and subcloning. Genomic DNA from selected clones was amplified and sequenced (Fig. 1b).
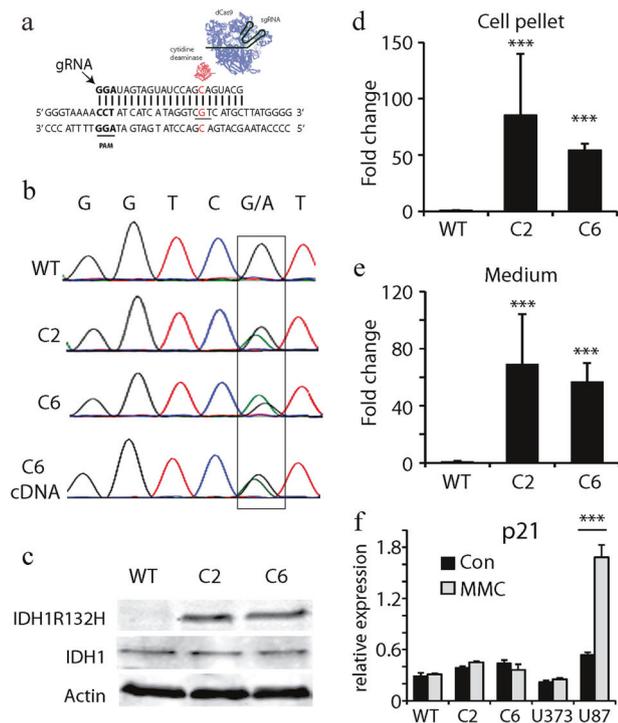
Fig. 1 Generating endogenous and heterozygous *IDH1* R132H mutation (*IDH1^{R132H/WT}*) in human astroglial cells. **a** Schematic illustration showing *IDH1* guide RNA (gRNA) sequence and the targeted strand using the "single base editing" technique with a fusion enzyme of catalytically dead Cas9 (dCas9) and cytidine deaminase. **b** Sanger sequencing of the PCR products of genomic DNA from an *IDH1* wild type clone (WT) and two heterozygous *IDH1^{R132H/WT}* clones (C2 and C6). The C2 and C6 showed a double peak with A/G reads at the edited G site. Same approach was used to sequence the PCR product from cDNA of C6 cells. **c** Immunoblotting with a specific antibody against IDH1 R132H (Mut IDH1) and an antibody recognizing both wild type and IDH1 R132H confirmed the expression of IDH1 in all three cell lines, but the IDH1 R132H protein was only detected in C2 and C6 cells. **d**, **e** Mass spectrometry was used to measure *IDH1^{R132H/WT}* oncometabolite 2-HG in both cell pellets (**d**) and conditioned media (**e**) of *IDH1* WT and two *IDH1^{R132H/WT}* clones. Endogenous *IDH1^{R132H/WT}* significantly increased 2-HG level in both the pellets and conditioned media of C2 and C6 cells (error bars stand for standard deviation). **f** SVG *IDH1* WT cells and *IDH1^{R132H/WT}* cells together with human glioblastoma U373 (with mutated *TP53*) and U87 (with wild type *TP53*) cells were treated with mitomycin C at 2.5 μg/ml for 4 h. RNA was collected for RT-PCR to detect p53 downstream target p21 expression. Following drug treatment, p21 was significantly elevated in U87 cells only, not in SVG *IDH1* WT and two *IDH1^{R132H/WT}* clones. ***$P < 0.001$

Compared with *IDH1* wild type cells (WT), two clones, named clone 2 (C2) and 6 (C6), showed double peaks with A/G reads at the edited site, indicating a heterozygous *IDH1* R132H point mutation in these clones (Fig. 1b). Most of the other clones harbored homozygous *IDH1* R132H mutation with an "A" read at the edited site (data not shown). In total, we sequenced 19 clones and four of them had heterozygous *IDH1* R132H mutation. The overall success rate of creating heterozygous *IDH1* R132H was ~20%.

The independently selected and expanded *IDH1^{R132H/WT}* clones C2 and C6 were maintained in medium for over 20 passages. We further examined the transcription of the two *IDH1* alleles by amplifying cDNAs from these cells followed by PCR and sequencing. Similarly, two peaks of A/G reads with similar abundance were observed at the edited site, indicating that these two *IDH1* alleles were equivalently transcribed (Fig. 1b).

Western blot analysis with a specific antibody against R132H IDH1 confirmed the expression of mutant IDH1 protein in C2 and C6 cells, but not in control cells (Fig. 1c). On the other hand, an antibody recognizing both wild type and R132H IDH1 detected IDH1 proteins in both WT and the two *IDH1^{R132H/WT}* clones (Fig. 1c).

To test the functionality of the edited *IDH1* gene in the two clones, cell pellets and conditioned media were collected for detection of the metabolic product of *IDH1^{R132H/WT}* 2-hydroxyglutarate (2-HG) by gas chromatography/mass spectrometry. Compared with control WT cells, 2-HG levels in the pellets from C2 and C6 cells were dramatically elevated by 55–85 fold (Fig. 1d, $P < 0.001$). The level of 2-HG in the conditioned media of C2 and C6 cells was also significantly higher than that of control (>57 fold, Fig. 1e, $P < 0.001$). These findings demonstrated that by employing "single base editing", we successfully created monoallelic *IDH1* R132H point mutation that faithfully recapitulates the naturally occurring heterozygous *IDH1^{R132H/WT}*, which encodes a functional chimeric IDH1 enzyme as evidenced by the production of its oncometabolite 2-HG.

Mutation/inactivation of the tumor suppressor gene *TP53* has been detected to co-exist with *IDH1* mutations in more than 80% of astrocytomas [2]. The SVG cells were immortalized with SV40 expressing large T antigen [14], which is well-known for its binding and inactivation of p53 protein [16]. To confirm that p53 was inactivated in our system, the cells were challenged with a DNA damage reagent mitomycin C (MMC). The expression level of p53 downstream target *p21* was examined by RT-PCR. MMC treatment for 4 h did not change the expression level of *p21* in either WT or the two *IDH1^{R132H/WT}* clones (Fig. 1f). In comparison, the same concentration of MMC induced significant increase in *p21* expression in human GBM U87 cells (>3 fold, $P < 0.001$), which harbor wild type *TP53* (Fig. 1f). Thus, we generated human astroglial models harboring both heterozygous *IDH1^{R132H/WT}* and p53 inactivation.

Global epigenetic alterations induced by *IDH1^{R132H/WT}* in astroglial cells

Mutant *IDH1* has been shown to trigger global epigenetic alterations [17, 18]. To investigate DNA methylation changes driven by *IDH1^{R132H/WT}* in our system, we
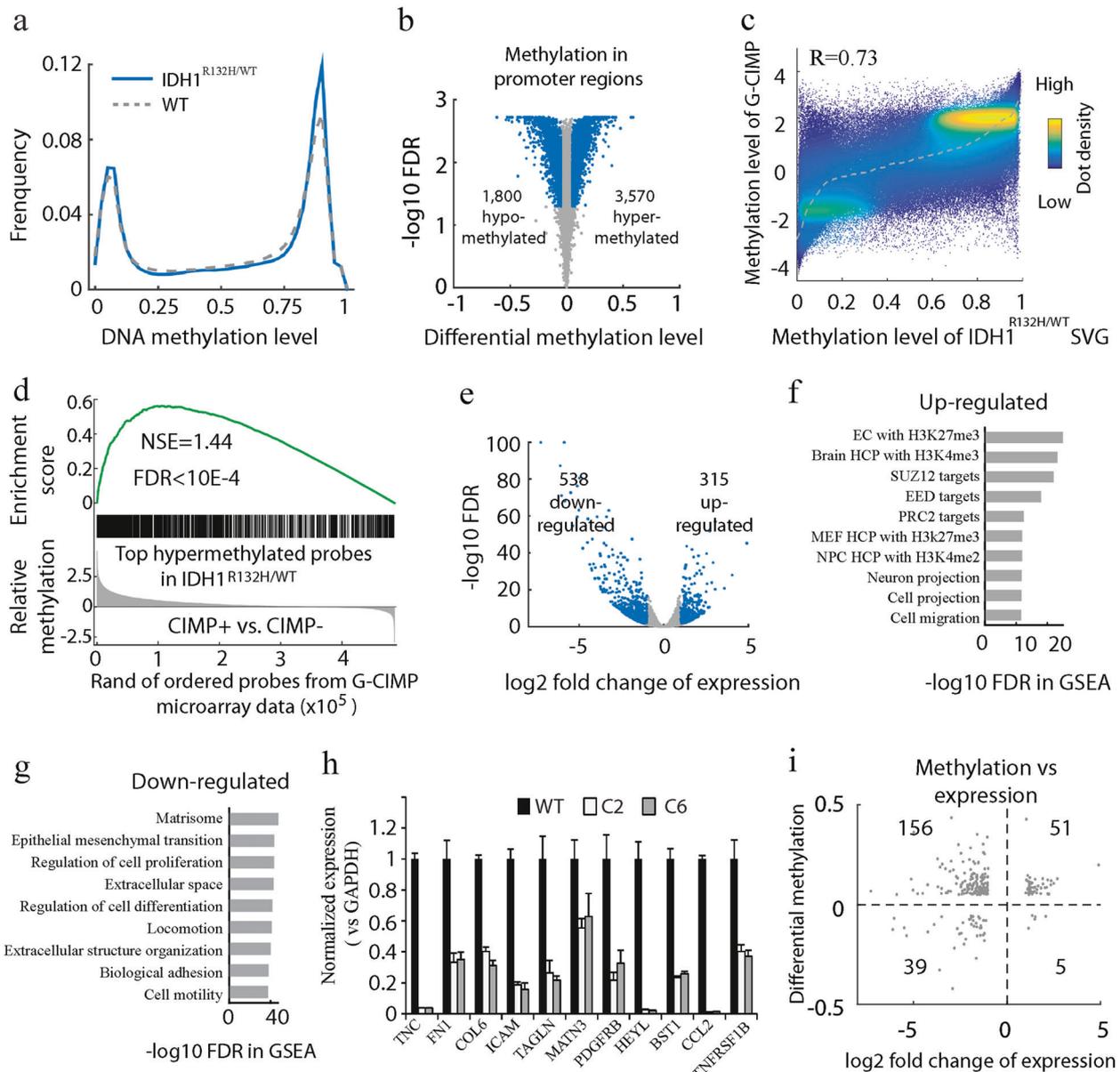
Fig. 2 DNA methylation and gene expression changes induced by $IDH1^{R132H/WT}$. **a** Comparison of methylation profiles showing relative DNA methylation distribution for WT and $IDH1^{R132H/WT}$ cells. Frequency (y-axis) is plotted against DNA methylation level (β, 0–1). Both $IDH1^{R132H/WT}$ clones showed increased frequency in high methylation levels (0.75–1). **b** About 21,647 CpG sites corresponding to 5370 gene promoter regions showed significant methylation alterations, among them ~3500 being hypermethylated, ~1800 hypomethylated in $IDH1^{R132H/WT}$ cells when compared with control cells. **c** Comparison of the methylation profiles between IDH1$^{R132H/WT}$ SVG and G-CIMP + tumors. The average methylation level of G-CIMP + tumor samples was used. The dash gray line indicates the average methylation level of G-CIMP+ in each bin of $IDH1^{R132H/WT}$ methylation. Pearson's correlation coefficient (R) is shown in the figure. **d** Gene set enrichment analysis (GSEA) of top hypermethylated probes in IDH1$^{R132H/WT}$ in G-CIMP tumors. Top 2,000 hypermethylated probes in IDH1 R132H/WT relative to wild type SVG (middle black bars) were used to perform GSEA. The green curve is the enrichment curve by comparison of top 2,000 hypermethylated probes in IDH1 R132H/WT to the ranked probes from G-CIMP microarray data (bottom gray bars). The probes from G-CIMP microarray data were ordered based on relative methylation level of CIMP+ to CIMP−. NES normalized enrichment score. FDR false discovery rate. **e** Global gene expression profiling in $IDH1^{R132H/WT}$ cells relative to the control cells. A total of 853 genes showed significant changes by $IDH1^{R132H/WT}$, 538 being downregulated, 315 being upregulated. **f** GSEA of upregulated genes indicated enrichment of PRC targets and cell migration pathways. **g** GSEA of upregulated genes indicated enrichment of cell proliferation, extracellular and cell motility pathways. **h** Quantitative real-time PCR (RT-PCR) validation of large scale RNA-sequencing analysis showed downregulation of genes involved in extracellular matrix proteins and cell proliferation pathway. All changes are significant. **i** A total of 251 genes were identified by overlapping differentially expressed genes and differentially methylated promoter regions from RNA-seq and methylome datasets, respectively. Based on methylation and gene expression changes, four groups of genes were plotted

performed genome-wide methylation profiling using Illumina Infinium Methylation EPIC Chip (850 K), which interrogates the methylation status of 850,000 CpG sites with comprehensive genome-wide coverage. Control SVG cells and $IDH1^{R132H/WT}$ cells had very different methylation profiles (Supplemental Fig. 2a), whereas C2 and C6 had similar methylation profiles (Supplemental Fig. 2b).Comparison of the relative methylation level distribution (β value, 0–1) revealed an increase in the frequency of CpG sites with high levels of methylation (β: 0.75–1) in $IDH1^{R132H/WT}$ cells (Fig. 2a), consistent with a hypermethation phenotype induced by $IDH1^{R132H/WT}$ [18]. On the genome scale, we identified 261,131 CpG sites with significant methylation alterations (hyper- or hypomethylated) between WT and $IDH1^{R132H/WT}$ cells. Among them, 21,647 CpG sites fall into the promoter regions of 5,370 genes. Two thirds of these promoter regions (3570, 66.5%) are hypermethylated by $IDH1^{R132H/WT}$, one third hypomethylated (Fig. 2b).

We compared the methylation profile of SVG $IDH1^{R132H/WT}$ cells with that of G-CIMP gliomas published by Turcan et al. [18]. The result indicated that there were highly correlated methylation profiles between our system and the G-CIMP tumors (Fig. 2c). Meanwhile, we performed gene set enrichment analysis (GSEA) and observed that the hypermethylated probes in SVG $IDH1^{R132H/WT}$ cell were significantly enriched in the hypermethylated probes from G-CIMP tumors (false discovery rate < 10E-4, Fig. 2d). All these suggest that our $IDH1^{R132H/WT}$ model generated by "single base editing" recapitulates the biological function of mutant IDH1 in gliomas.

Global genetic alterations driven by $IDH1^{R132H/WT}$

To investigate global gene expression changes induced by $IDH1^{R132H/WT}$, we performed RNA-sequencing (RNA-seq) analysis. A comparison of the expression profiles between replicates showed high reproducibility (Supplemental Fig. 3a, b). Global gene expression analysis identified 315 genes were significantly upregulated by $IDH1^{R132H/WT}$, and 538 downregulated (Fig. 2e). Pathway analysis of the 315 upregulated genes found enrichment of targets of polycome repression complex 2 (PRC2) as well as genes involved in cell projection and cell migration (Fig. 2f). On the other hand, pathway analysis of the downregulated genes revealed that cell proliferation, differentiation, ECM components, extracellular space, and structure organization were inhibited by $IDH1^{R132H/WT}$ (Fig. 2g and Supplemental Table 1).

Quantitative RT-PCR (qRT-PCR) analysis validated that $IDH1^{R132H/WT}$ decreased the expression of many ECM components in SVG cells, including tenascin C (TNC), fibronectin (FN1), collagen type IV and VI (COL6) (Fig. 2h), consistent with our RNA-seq analysis. We also validated the expression of a subset of genes in the cell proliferation pathway and confirmed that $IDH1^{R132H/WT}$ decreased the expression of platelet-derived growth factor receptor beta (PDGFRB) and HES-related family BHLH transcription factor with YRPW motif-like (HEYL) (Fig. 2h). Most of these downregulated genes by $IDH1^{R132H/WT}$ were rescued by treatment with a potent and selective mutant IDH1 inhibitor AGI-5198 (Supplemental Fig. 3c), which lowered the level of 2-HG in C2 and C6 cells to that of control cells (data not shown). This confirms that mutant IDH1 created by "single base editing" regulates gene expression via its oncometabolite production.

To identify genes regulated via a DNA methylation-dependent mechanism by $IDH1^{R132H/WT}$, we overlapped our DNA methylome with RNA-seq dataset and generated a list of 251 genes with both promoter methylation changes and gene expression alterations. We grouped the 251 genes into 4 categories (Fig. 2i), namely downregulated with promoter hypermethylation (156 genes, 62%, Supplemental Table 2 and supplemental Fig. 4a); upregulated with promoter hypermethylation (51 genes, 20%, Supplemental Table 3), downregulated with promoter hypomethylation (39 genes, 15%) and upregulated with promoter hypomethylation (5 genes) (Supplemental Table 4).

From our analysis, we found that many metabolic enzymes were downregulated by $IDH1^{R132H/WT}$ via promoter hypermethylation, including acyl-CoA dehydrogenase (ACADS), Aldehyde Dehydrogenase 2 Family (ALDH2), and Aldehyde Oxidase 1 (AOX1). There were a total of 51 genes upregulated by $IDH1^{R132H/WT}$ with promoter hypermethylation. Pathway analysis of this group revealed that many of them were PRC2 or SUZ12 targets (Supplemental Fig. 4b), suggesting that histone modifications were involved in gene regulation in the presence of promoter methylation. We further interrogated overall histone methylation changes induced by $IDH1^{R132H/WT}$. Most of the surveyed histone marks, including H3K27me3, H3K36me3, and H3K4me3, were decreased in $IDH1^{R132H/WT}$ cells. The repressive histone mark H3K9me3 was increased in C2 and C6 cells relative to control (Supplemental Fig. 4c). In all, the epigenetic and genetic analyses of our isogenic cellular system harboring heterozygous $IDH1^{R132H/WT}$ provide a plethora of data to identify the molecular targets and pathways altered by $IDH1^{R132H/WT}$.

Edited $IDH1^{R132H/WT}$ promotes cell migration

In our RNA-seq analysis, we found many ECM-related pathways were downregulated by $IDH1^{R132H/WT}$ (Fig. 2g), we investigated the effect of $IDH1^{R132H/WT}$ on migration and invasion of SVG cells. Transwell assays revealed that after
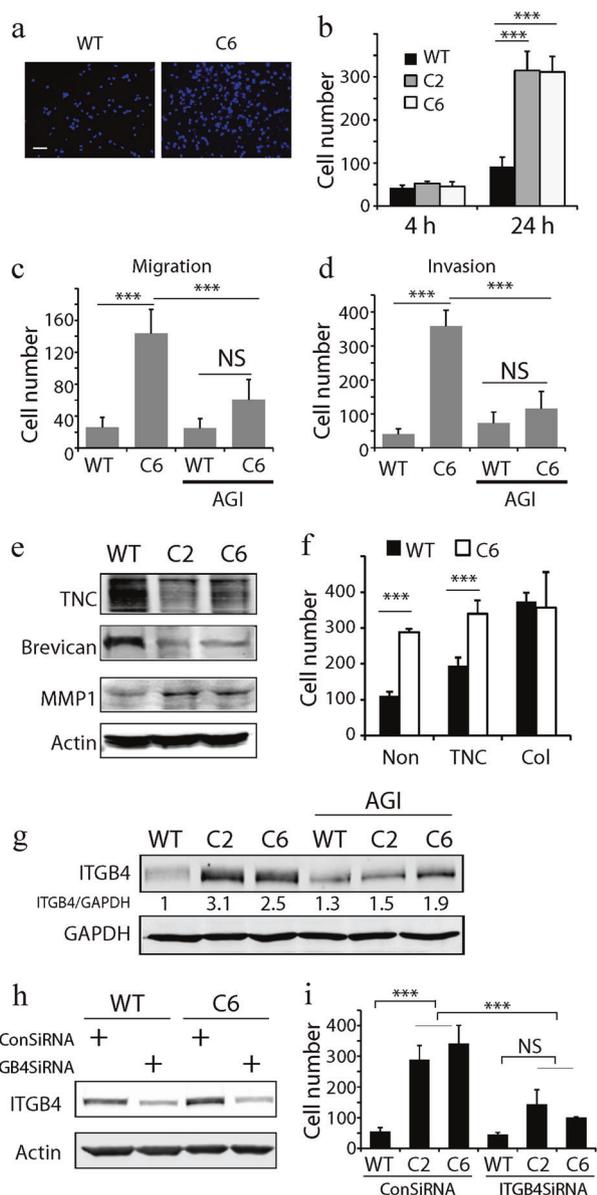
Fig. 3 Endogenous *IDH1*^R132H/WT^ promotes cell migration and invasion via a 2-HG-dependent mechanism. **a** Microphotograph of migrated cells on transwell membrane 24 h after plating. Bar = 100 μm. **b** Cell counting of migrated cells at 4 h and 24 h after plating. **c** AGI-5198 had no effect on WT cell migration, but completely blocked the pro-migratory effect of *IDH1*^R132H/WT^ in C2 cells. **d** Cell invasion assays on matrigel-coated transwells also showed that *IDH1*^R132H/WT^ dramatically increased cell invasion by more than sevenfold, which was completely reversed by AGI-5198. **e** Western blot analysis revealed decrease in extracellular matrix proteins and increase in MMP1 in *IDH1*^R132H/WT^ cells. **f** Transwell assays of SVG IDH1 WT and *IDH1*^R132H/WT^cells plated on non-coated (non), TNC or collagen-coated surfaces. **g** Western blotting analysis showed 2.5–3 fold increase in ITGB4 by *IDH1*^R132H/WT^, which was reversed by AGI-5198 (1.5 μmol/L). **h** Compared with control siRNA, ITGB4 specific siRNA downregulated ~50% ITGB protein expression in both SVG IDH1 WT and *IDH1*^R132H/WT^cells. **i** ITGB4 knockdown dramatically decreased cell migration induced by *IDH1*^R132H/WT^ in transwell assays (***$P <$ 0.001)

plating for 4 h, there was no difference in cell migration between control and *IDH1*^R132H/WT^ cells. Yet, 24 h after plating, there was a ~3-fold increase in cell migration in *IDH1*^R132H/WT^ clones (Fig. 3a, b, $P < 0.001$). The pro-migratory effect of *IDH1*^R132H/WT^ was completely blocked by AGI-5198 (Fig. 3c). In addition, we performed invasion assays using matrigel-coated transwells. *IDH1*^R132H/WT^ dramatically increased cell invasion by more than sevenfold, which was completely reversed by AGI-5198 (Fig. 3d). These results suggest that the pronounced cell migratory and invasive capacity of *IDH1*^R132H/WT^ cells is 2-HG dependent.

To understand the molecular mechanism of the pro-migratory role of *IDH1*^R132H/WT^ in SVG cells, we searched a few cell migration-related targets from our RNA-seq analysis. Consistent with our RNA-seq analysis, Western blotting analysis found a decrease in TNC and an increase in matrix metalloproteinase-1 (MMP1) in *IDH1*^R132H/WT^ cells (Fig. 3e). Since disrupted ECM would make it easier for cells to migrate, we examined cell migration on ECM protein-coated surfaces. Cell migration on TNC or collagen-coated transwells increased in both control and *IDH1*^R132H/WT^ cells (Fig. 3f), suggesting that the decreased ECM components cannot explain the pro-migratory role of *IDH1*^R132H/WT^.

Our gene ontology analysis showed that *IDH1*^R132H/WT^ unregulated cell migration pathway. Integrin β 4 (ITGB4), a receptor subunit for laminin, was upregulated ~3-fold by *IDH1*^R132H/WT^ at the mRNA level. Our Western blotting analysis confirmed elevation of ITGB4 by ~2.5–3-fold at the protein level, which was reversed by AGI-5198 (Fig. 3g). We performed loss-of-function studies using ITGB4 siRNA, which downregulated 50% of ITGB4 expression (Fig. 3h). Transwell assays revealed that the cell migration induced by *IDH1*^R132H/WT^ was significantly reversed by knocking down ITGB4 (Fig. 3i). Thus, ITGB4 is involved in the pro-migratory role of *IDH1*^R132H/WT^.

Edited *IDH1*^R132H/WT^ decreases cell growth

Our RNA-seq data also revealed downregulation of cell proliferation pathways by *IDH1*^R132H/WT^ (Fig. 2g), we investigated how *IDH1*^R132H/WT^ affected the growth of SVG cells. Compared with control, *IDH1*^R132H/WT^ cells were less proliferative. Relative to WT cells, there were ~55% fewer cells in C2 and C6 cultures on day 4 and 6 (Fig. 4a, $P < 0.001$). To examine if the oncometabolite 2-HG mediated the anti-proliferative role of *IDH1*^R132H/WT^, cells were treated with the mutant IDH1 inhibitor. AGI-5198 had no effect on *IDH1* WT cell growth [$(5.65 \pm 0.42) \times 10^5$ vs. $(4.74 \pm 0.28) \times 10^5$], but completely rescued the cell number loss in *IDH1*^R132H/WT^ cells, [from $(2.88 \pm 0.11) \times 10^5$ to $(4.5 \pm 0.39) \times 10^5$, Fig. 4b, $P < 0.001$], further confirming that
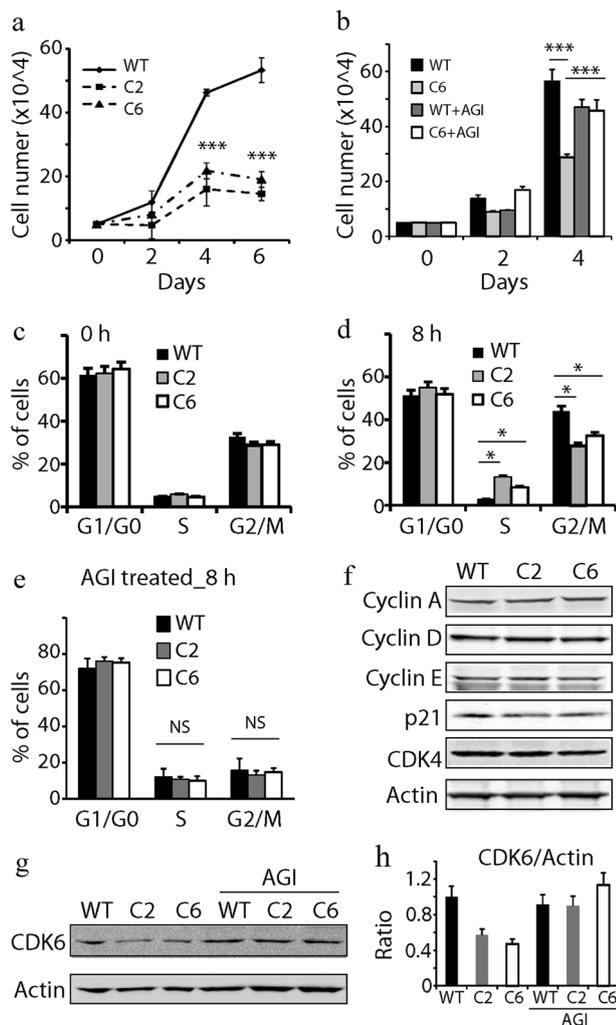
Fig. 4 *IDH1*[R132H/WT] decreases cell proliferation via a 2-HG dependent manner. **a** Cell growth curves of control, C2 and C6 cells. Cells were plated into 6-well plates at 5×10^4 and counted every 2 days. At day 2, there was no significant difference in cell growth. At day 4 and day 6, there were ~55–65% less cells in C2 and C6 cultures compared with control. **b** Both WT and C6 Cells were incubated with the mutant IDH1 inhibitor AGI-5198 or vehicle DMSO for 2 weeks prior to the cell growth analysis. AGI-5198 had no effect on WT cell growth on day 4, but completely rescued cell number loss in C6 cells. **c**, **d** Cell cycle analysis. Cells were plated at 2×10^5 in 6 cm dishes and grew in 10% serum containing medium for 24 h followed by incubation in 0.1% FCS medium for 36 h. Cells were then replenished with 10% serum and collected at indicated time point after serum addition for cell cycle analysis by flow cytometry/PI staining. Percentage of cells at different cell cycle phase before (0 h, **c**) and 8 h (**d**) after serum replenishing were plotted. **e** Cells were treated with AGI-5198 and analyzed 8 h after serum repletion followed by cell cycle analysis. **f–h** Western blot analysis of cell cycle regulators indicated decrease in CDK6 by *IDH1*[R132H/WT], which was rescued by AGI-5198 treatment ($*P < 0.05$, $***P < 0.001$)

IDH1[R132H/WT] inhibited astroglial cell proliferation via its oncometabolite production.

Cell cycle progression was analyzed after cells were synchronized by serum withdrawal for 36 h. Right after

synchronization, ~60% of the cells were arrested at G0/G1 phase, ~30% of the cells stayed at G2/M phase, and only a small percentage of the cells were at S phase (~4%) in both control and the two *IDH1*[R132H/WT] clones (Fig. 4c, 0 h). After adding serum for 8 h, WT cells decreased from 60% to 51% at G1/G0 phase, increased from 32 to 44% at G2/M phase and slightly down to 2% at S phase, suggesting that WT cells quickly progressed to G2/M phase after serum stimulation (Fig. 4d, 8 h). In comparison, the *IDH1*[R132H/WT] cells showed the same degree of decrease at G1/G0 phase (from 64% to 52%); but there was no increase in G2/M phase. Instead, *IDH1*[R132H/WT] cells accumulated at S phase from 4% to 8–13% after serum replenishing (Fig. 4d). Our data indicated that *IDH1*[R132H/WT] decreased cell growth by delaying cell progression from S to G2/M phase. We performed cell cycle analysis for up to 32 h after serum stimulation and found similar patterns of cell cycle difference between the control and *IDH1*[R132H/WT] cells (Supplemental Fig. 5a-c). Moreover, the blocked S phase in *IDH1*[R132H/WT] cells was reversed by AGI-5189 (Fig. 4e). We further analyzed the protein level of cell cycle regulators. No dramatic change in cyclin A, D, E, p21 and cyclin-dependent kinase 4 (CDK4) was found in our system (Fig. 4f). A decrease (~40–50%) in CDK6 was detected in *IDH1*[R132H/WT] cells, which was rescued by AGI-5189 (Fig. 4g, h).

Cell proliferation pathways regulated by *IDH1*[R132H/WT]

Next we focused on molecular targets and signaling transduction pathways responsible for the profound cell growth rate change in *IDH1*[R132H/WT] cells. Western blot analysis showed that many cell proliferation signaling pathways, including MAPK, Notch, and Wnt, were repressed by *IDH1*[R132H/WT]. For example, phosphorylation of three MAPK members, e.g. ERK1/2, JNK, and p38, were downregulated by 40, 20%, and 40–60% in *IDH1*[R132H/WT] cells, respectively (Fig. 5a). The Notch ligand Jagged 1 was decreased by more than 80% in *IDH1*[R132H/WT] cells. The protein level of NOTCH1 receptor was not altered by *IDH1*[R132H/WT]; however, the cleaved form of NOTCH1, NICD1, decreased by 42% in C2 and C6 cells (Fig. 5b). We also found β-catenin, the effector of the Wnt pathway, was downregulated by more than 40% in *IDH1*[R132H/WT] cells (Fig. 5c). In contrast, the AKT pathway was not changed by *IDH1*[R132H/WT] (Fig. 5c).

The effectors of Hippo pathway, Yes-associated protein (YAP) and transcriptional coactivator with a PDZ-binding domain (TAZ), were also examined. YAP protein was highly expressed in WT cells, but was ~50% downregulated in C2 and C6 *IDH1*[R132H/WT] cells (Fig. 5d). In contrast, the expression level of TAZ was not changed by *IDH1*[R132H/WT]
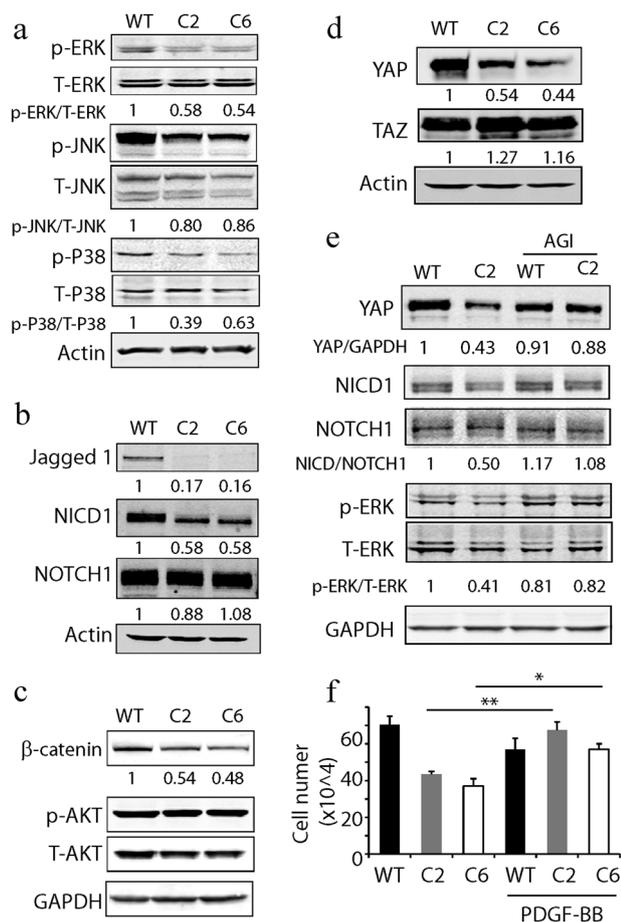
Fig. 5 Cell proliferative pathways altered by *IDH1*^{R132H/WT}. **a** Phosphorylation of three MAPK members, namely ERK1/2, JNK, and p38, were downregulated by *IDH1*^{R132H/WT}. **b** Immunoblotting analysis of control, C2 and C6 cells revealed that Jagged 1 and NICD1 was downregulated by *IDH1*^{R132H/WT}. The NOTCH1 receptor was not affected by *IDH1*^{R132H/WT}. **c** The effector of Wnt pathway β-catenin was downregulated in C2 and C6 cells; *IDH1*^{R132H/WT} did not alter the AKT pathway. **d** YAP protein was highly expressed in WT cells and was downregulated by ~50% in C2 and C6 *IDH1*^{R132H/WT} cells. The expression level of TAZ was not decreased by *IDH1*^{R132H/WT}. **e** AGI-5198 completely rescued *IDH1*^{R132H/WT}-mediated decrease in YAP, NICD1, and p-ERK1/2 pathways. **f** Cells were treated with PDGF-BB (30 ng/ml) in normal culture medium for 4 days. PDGF-BB significantly increased cell proliferation in C2 and C6 SVG *IDH1*^{R132H/WT} cells but not in SVG *IDH1* WT cells (*$P < 0.05$, **$P < 0.01$)

(Fig. 5d), indicating that the decreased YAP expression was independent of the Hippo pathway.

The downregulation of YAP, NICD1, and p-ERK1/2 by *IDH1*^{R132H/WT} was completely reversed by the mutant IDH1 inhibitor AGI-5198 (Fig. 5e), corroborating with a dominant role of 2-HG in repressing these cell proliferation pathways.

Next, we evaluated the involvement of the PDGF-PDGFR pathway in *IDH1*^{R132H/WT} cells, since PDGF signaling has been implicated in IDH-mutant glioma biology. Consistent with findings from Flavahan et al. [19], our

RNA-seq data showed upregulation of PDGFRA by *IDH1*^{R132H/WT}. On the other hand, our RNA-seq also found dramatic downregulation of PDGFRB by 48% in *IDH1*^{R132H/WT} cells, which was confirmed by our qRT-PCR analysis (Fig. 2h). To determine whether PDGF-PDGFR pathway is involved in the anti-proliferative function of *IDH1*^{R132H/WT}, we challenged the cells with exogenous PDGF-BB, which binds to both PDGFRA and PDGFRB. Proliferation in C2 and C6 cells was significantly increased by PDGF-BB, but not in control cells (Fig. 5f). Our results indicate that downregulation of the PDGF-PDGFR signaling pathway is involved in the growth defect of SVG *IDH1*^{R132H/WT} cells.

YAP mediates the anti-proliferative role of *IDH1*^{R132H/WT}

We want to identify novel targets of *IDH1*^{R132H/WT}. YAP plays an important role in cell proliferation [20]. Given the un-identified role of YAP in *IDH1*^{R132H/WT}-mediated biological function, we focused on the involvement of YAP signaling in *IDH1*^{R132H/WT}-mediated cell proliferation defect. A close look at our RNA-seq revealed *YAP* was 50% downregulated by *IDH1*^{R132H/WT} at the transcriptional level. We validated *YAP* expression by RT-PCR. In comparison to control cells, the mRNA level of *YAP* was decreased by more than 50% in C2 and C6 cells (Fig. 6a, $P < 0.001$). However, the methylation level of the CpG sites at *YAP* promoter regions did not change, indicating an epigenetic-independent gene regulation mechanism (Supplemental Fig. 6a). Immunocytochemistry studies showed that YAP protein was located in the cytosol and nucleus, and *IDH1*^{R132H/WT} decreased overall YAP expression in both of the cellular compartments (Fig. 6b).

To substantiate that YAP downregulation mediated the cell growth inhibition effect of *IDH1*^{R132H/WT}, control cells and *IDH1*^{R132H/WT} cells were transiently transfected with YAP expression vector or control vector. Immunoblotting analysis confirmed elevated YAP protein level (Fig. 6c, upper panel). Forced YAP expression in control cells did not affect cell growth [$(7.80 \pm 0.11) \times 10^5$ vs. $(7.00 \pm 0.10) \times 10^5$] (Fig. 6c, lower panel). In contrast, forced YAP expression in C2 *IDH1*^{R132H/WT} cells significantly rescued cell number loss induced by *IDH1*^{R132H/WT} from $(3.85 \pm 0.21) \times 10^5$ to $(5.70 \pm 0.41) \times 10^5$ (Fig. 6c, $P < 0.001$). Our data support that downregulation of YAP mediates the cell growth inhibition effect of *IDH1*^{R132H/WT} in SVG cells.

To determine the signaling transduction network of YAP pathway in *IDH1*^{R132H/WT} cells, we forced YAP expression and examined downstream effectors of YAP in *IDH1*^{R132H/WT} cells. Elevated YAP protein level increased the expression of Jagged 1, but not p-ERK1/2 and β-catenin, suggesting that Notch pathway, but not MAPK or Wnt, was
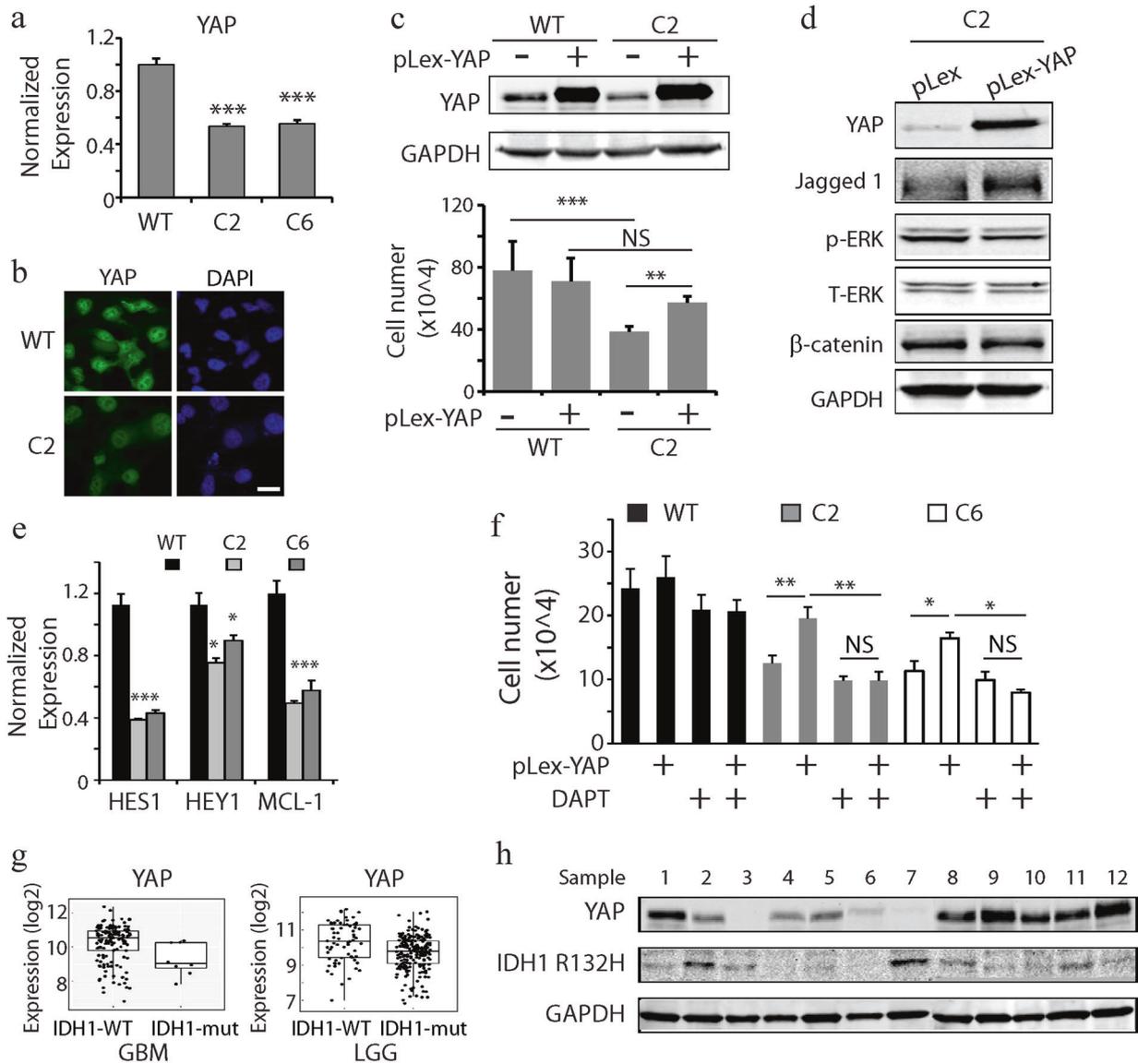
Fig. 6 *IDH1^{R132H/WT}* inhibited cell growth by downregulating YAP expression. **a** RT-PCR indicated that the mRNA level of YAP was decreased by more than 50% in C2 and C6 cells when compared with WT cells. **b** Immunocytostaining of YAP protein in WT and C2 cells. YAP was expressed in both cytosol and nucleus. *IDH1^{R132H/WT}* decreased overall YAP expression in both cytosol and nucleus. Bar = 20 μm. **c** YAP mediated the cell growth inhibition effect of *IDH1^{R132H/WT}*. WT and C2 cells were transiently transfected with a YAP expression plasmid and a control vector pLex. Cells were counted at 4 days after transfection. **d** Identification of downstream targets of YAP in *IDH1^{R132H/WT}* cells. C2 cells were transiently transfected with the YAP expressing plasmid and the control vector. After 48 h, proteins were collected for immunoblotting. Elevated YAP increased Jagged 1, but not p-ERK or β-catenin, indicating that the Notch pathway was downstream of YAP. **e** The effectors of Notch pathway *HES1* and *HEY1* were significantly decreased in C2 and C6 clones. YAP downstream target *MCL-1* was also downregulated in C2 and C6 cells. **f** Cells were treated with the Notch pathway inhibitor DAPT (2 μmol/L) for 30 min prior to YAP or empty vector transfection. Cell number was counted 3 days after transfection. **g** Analysis of TCGA data indicated that compared with IDH1 WT tumors, YAP expression level was significantly lower (*P* < 0.05) in IDH1-mutant glioblastomas (left) and low grade gliomas (LGG, right). **h** A survey of 12 primary glioma neurosphere cultures derived from patient samples by immunoblotting with anti-YAP and anti-mutant IDH1 R132H antibodies indicated that IDH1 R132H status was moderately correlated with low YAP protein expression ($R^2 = 0.38$). (*$P < 0.05$, **$P < 0.01$, ***$P < 0.001$)

downstream of YAP signaling in *IDH1^{R132H/WT}* cells (Fig. 6d). Furthermore, the mRNA level of two common downstream targets of Notch pathway, *HES1* and *HEY1*, was significantly decreased by 64% ($P < 0.001$) and 27% ($P < 0.05$) in *IDH1^{R132H/WT}* cells, respectively (Fig. 6e). Another

downstream target of YAP, *MCL-1*, was also significantly decreased (>50%) by *IDH1^{R132H/WT}* at the mRNA level (Fig. 6e). The downregulation of the examined Notch pathway targets was reversed by AGI-5198 treatment (Supplemental Fig. 6b). To further examine the relationship between the

YAP and Notch pathways, we pre-treated the C2 and C6 *IDH1^{R132H/WT}* cells with a potent Notch pathway inhibitor DAPT [21] prior to forced YAP expression. DAPT significantly reversed the growth-promoting effect of YAP gain-of-function (Fig. 6f), further supporting our conclusion that Notch is downstream of YAP to mediate the anti-proliferative role of *IDH1^{R132H/WT}*.

To determine the upstream signaling that regulate YAP, we first examined Wnt pathway because it has been reported that the transcription factor β-catenin bound to enhancers to directly regulate YAP expression [22]. When the C2 cells were treated with a cell permeable and selective Wnt signaling pathway agonist 1 (Wnt A1) for 24 h, the effector of Wnt pathway, β-catenin, was elevated (Supplemental Fig. 6c). However, YAP protein level was not rescued by Wnt agonist 1 in C2 cells (Supplemental Fig. 6c), suggesting that the Wnt pathway is not upstream of YAP.

Finally, we determined if the reverse correlation between *IDH1^{R132H/WT}* and *YAP* was true in human GBM samples, we queried YAP expression in GBM and low grade gliomas (LGG) from TCGA database and found that YAP expression level is significantly lower in IDH1 mutant gliomas compared with that in IDH1 WT gliomas in both the GBM and LGG category (Fig. 6g $P < 0.05$). Moreover, compared with classic and mesenchymal GBM, *YAP* mRNA level is significantly lower in proneural GBM, which is characterized by mutations in *IDH1/2* and alterations in PDGFRA [23] (Supplemental Fig. 6d, $P < 0.05$). As the *IDH1* mutation is sufficient to establish the glioma hypermethylator phenotype (G-CIMP) [18], we compared *YAP* mRNA levels in G-CIMP and non G-CIMP gliomas. Again, *YAP* expression is significantly lower in G-CIMP tumors (Supplemental Fig. 6e, $P < 0.05$). Furthermore, we examined YAP and R132H IDH1 protein expression in 12 primary human glioma neurosphere cell lines derived from patient samples (Fig. 6h). R132H IDH1 expression was found moderately correlated with low YAP protein expression ($R^2 = 0.38$), substantiating our in vitro studies. Thus, with our unique isogenic *IDH1^{R132H/WT}* models, we identified YAP as a novel downstream target of *IDH1^{R132H/WT}*.

We also tested the tumor formation ability of *IDH1^{R132H/WT}* + p53 inactivated human astroglial cells in immunodeficient (SCID) mice. Neither the control cells nor the *IDH1^{R132H/WT}* cells formed subcutaneous or intracranial tumors after 6 month of implantation (data not shown), suggesting that additional gene mutations may be needed to transform these cells.

Discussion

In this work, we employed the highly efficient "C to T" single base editing approach to create cell lines harboring heterozygous *IDH1^{R132H/WT}*. The edited *IDH1* gene recapitulates the biological function of the naturally occurring monoallelic IDH1 R132H mutation by demonstrating 2-HG-dependent genotype and phenotype changes. Using the isogenic cellular system that differ only in a nucleotide in one allele of the *IDH1* gene, we further identified molecular targets and pathways affected by *IDH1^{R132H/WT}*. Among them, YAP functions as a novel downstream target of *IDH1^{R132H/WT}* to mediate the anti-proliferative role of *IDH1^{R132H/WT}*. We also found that YAP expression inversely correlated with *IDH1^{R132H/WT}* in human glioma samples. Our findings may explain the clinical observations that brain tumor patients with mutant IDH1 survive longer and respond better to therapies when compared with those harboring IDH1 wild type. Thus, the robust "single base editing" approach opens up an efficient way to create isogenic cellular models harboring heterozygous IDH1 mutations for functional and molecular mechanistic study of mutant IDH1.

Until recently, most functional studies of mutant IDH1 rely on exogenous overexpression systems, partially due to the difficulties involved in obtaining cell lines from low-grade gliomas, or growth disadvantage of cells carrying *IDH1* mutations in vitro. Using genome editing to generate heterozygous *IDH1* mutations has been sparsely explored by others. Works from Duncan et al. [17] and Ma et al. [24] have employed recombinant genomic techniques and TALEN/zinc finger to knock in or knock out *IDH1* mutations in cancer cells. Recently, Sulkowski et al. [25] employed CRISPR/Cas9 and single-stranded donor DNA to generate cancer cell lines with heterozygous *IDH1^{R132H/WT}*. Compared with other genome editing techniques, the "single base editing" technique used in our current study has a high success rate (~20% for the heterozygous editing), which can greatly reduce the time and effort to establish isogenic cellular models for mutant IDH1 studies. Given the prevalence of *IDH1* mutations in many other cancer types, our strategy provides a valuable tool for the IDH1 research community and can be readily tested in other cell systems.

Our genome-wide DNA methylation profiling revealed that *IDH1^{R132H/WT}* mainly induced hypermethylator phenotype in our system, consistent with findings from others [17, 18]. While the mechanism of *IDH1^{R132H/WT}*-mediated hypermethylation is well described, the molecular basis of *IDH1^{R132H/WT}*-mediated hypomethylation requires further investigation. Global DNA methylation will affect gene expression changes. In general, promoter hypermethylation is associated with gene silencing. However, in our list of 251 genes, only 156 genes followed this traditional model of methylation-dependent gene repression. Other mechanisms, e.g. insulator dysfunction may be involved in gene activation with promoter hypermethylation [19]. Moreover,
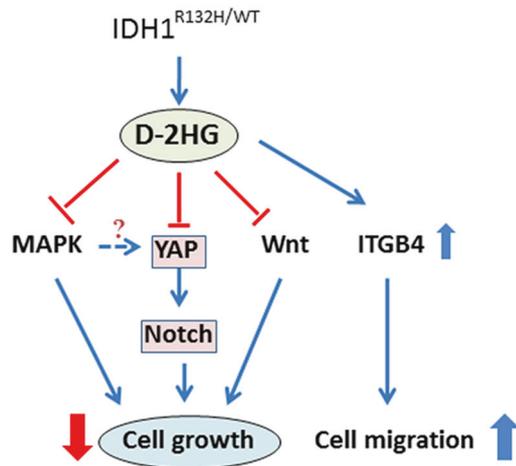
Fig. 7 Schematic illustration of molecular and cellular events induced by endogenous *IDH1*$^{R132H/WT}$ in human astroglial cells with p53 inactivation

recent studies, including our own, suggested that DNA hypermethylation in promoter regions could recruit histone modifications and lead to gene activation [26]. In the *IDH1*$^{R132H/WT}$ cells, the same mechanism may be implicated in gene activation in the presence of promoter hypermethylation. For example, our pathway analysis identified many activated genes as targets of the PRC complex, which mediates the repressive histone mark H3K27me3. Since DNA methylation has been previously reported to reversely correlate with H3K27me3 [27], it is tempting to speculate that a decrease in H3K27me3 following promoter hypermethylation could result in gene activation. In fact, in our global analysis of histone mark changes, most of the repressive histone marks were found decreased in *IDH1*$^{R132H/WT}$ cells. Our data suggest that although 2-HG inhibits several histone demethylases, *IDH1*$^{R132H/WT}$ does not always result in an increase in histone methylation [18]; for example, others have reported no change in histone methylation in orthotropic xenografts [28].

There is no doubt that the biological function of *IDH1*$^{R132H/WT}$ is contextually dependent. Both pro-and anti-migratory roles of *IDH1*$^{R132H/WT}$ have been recorded [29, 30]. Corroborating with other in vitro and in vivo studies [30, 31], our cellular phenotype analysis indicated a dramatic increase in the migratory ability of *IDH1*$^{R132H/WT}$ cells. Most of the pro-migratory signaling pathways, e.g. MAPK, YAP, Notch, AKT, were either downregulated or unchanged in our system. Many ECM proteins were also downregulated by *IDH1*$^{R132H/WT}$, which is consistent with studies for others [32]. In our unbiased large scale gene expression analysis and immunoblotting analysis, we found that ITGB4 is involved in the pro-migratory role of *IDH1*$^{R132H/WT}$. Future mechanistic investigation will help to elucidate whether the pro-migratory role of *IDH1*$^{R132H/WT}$ is

one of the driving forces of *IDH1*$^{R132H/WT}$-mediated cell transformation during oncogenesis.

Similarly, both anti- and pro-proliferative roles of IDH1 R132 H have been reported [33, 34]. In our models, we found *IDH1*$^{R132H/WT}$ triggered a profound cell growth inhibition. Most of the cell proliferation-related signaling pathways, including MAPK, Notch, Wnt, and YAP, were downregulated by *IDH1*$^{R132H/WT}$. The Hippo pathway effector YAP is a major regulator of organ size and proliferation in vertebrate. In some tissues, YAP acts as an oncogene but in other tissues YAP functions as a tumor suppressor [35]. In our system, we identified Notch pathway downstream of YAP, consistent with the work from Tschaharganeh [36]. Since YAP promoter was not hypermethylated in *IDH1*$^{R132H/WT}$ cells when compared to control, the mechanism of YAP downregulation by *IDH1*$^{R132H/WT}$ requires more detailed studies. Schematic of the signaling network and cellular phenotypes regulated by *IDH1*$^{R132H/WT}$ in human astroglial cells is shown in Fig. 7. It is worthy to note that even though the anti-proliferative role of mutant IDH1 has been reported by others and us, the genetic evidence that IDH mutation is required for gliomagenesis is profound. It is conceivable that *IDH1*$^{R132H/WT}$ may provide some sort of proliferative advantage in the right cell-of-origin such as neural stem cells or oligodendrocyte progenitor cells. Another possibility is that *IDH1*$^{R132H/WT}$ may impair/inhibit biological mechanisms required for direct malignant transformation, yet still enable more indolent tumorigenesis, such as alteration of the interaction between pre-cancerous cells and immune cells.

In summary, this work highlights what we believe to be a novel approach of generating isogenic cellular models of monoallelic *IDH1* R132H point mutation with high efficiency. However, we noticed the limitation of our current cell model. The SVG cells do not form intracranial or subcutaneous tumors in animals *per se*; changing *IDH1* status in this model was not adequent to drive tumor formation either. Our in vivo study suggests that either additional genetic alteration is required to transform the SVG cells; or the order of *IDH1* and *TP53* mutation is critical for tumorigenesis. This limitation, however, did not diminish the implication of our findings. In the future, we will apply this gene editing strategy to other cellular systems to fully assess the biological function of *IDH1*$^{R132H/WT}$ in tumorigenesis and tumor response to therapies.

Materials and Methods

Reagents and Cell Cultures

All reagents were purchased from Sigma-Aldrich (St Louis, MO) unless otherwise stated. The human astroglial cell line

SVG-10B1 was originally established by Dr. Major [14, 15] and obtained via a material transfer agreement. Human GBM U87 and U373 cells were original purchased from ATCC. All cell lines are free of mycoplasma and authenticated with short tandem repeat profiling by Johns Hopkins Genetic Resources Core facility using Promega GenePrint 10 system (Madison, WI). SVG cells were cultured in Dulbecco's Minimum Essential Media (DMEM, Thermo Fisher Scientific, Grand Island, NY) supplemented with 10% fetal calf serum (FCS, Gemini Bio-products, West Sacramento, CA). Cells were incubated in a humidified incubator containing 5% CO_2/95% air at 37 °C, and passaged every 2–4 days.

The mutant IDH1 inhibitor AGI 5198 was purchased from Selleckchem (Houston, TX) and used to treat the cells at 1.5 µmol/L for 2 weeks; MMC at 2.5 µg/ml for 4 h, Wnt agonist 1 (Selleckchem) at 1 µmol/L overnight.

Single base editing

We applied the method from Komor et al. [13] to generate heterozygous *IDH1* gene with a point mutation at R132H (CGT → CAT) in human astrocytes. The gRNA was chosen by using an online tool developed by Zhang' Lab (http://crispr.mit.edu/) with the sequence of 5′-GCAUGACGACCUAUGAUGAUAGG-3′. The Guide RNA was cloned into a cloning vector (Addgene, 41824) using Gibson assembly mix (New England Biolabs, Ipswich, MA). The gRNA was validated by transfecting human embryonic kidney 293FT cells with the gRNA vector and a wild type Cas9 plasmid (pCas9-EGFP, Addgene) using Lipofectamine 3000 (Invitrogen, Carlsbad, CA). Two days after transfection, genomic DNA was extracted from these cells and amplified using the primers: F: 5′-AGAATCGTGATGCCACCAAC-3′; R: 5′-TGCATTTCTCAATTTCATACC TTG-3′. The precise cut of Cas9 with the guidance of the gRNA was validated by using T7EI assay (New England Biolabs).

For "single base editing", 2×10^5 cells per well were seeded in 6-well plate and co-transfected with gRNA plamid and pCMV-BE3 plasmid (Addgene,73021) with Lipofectamine 3000. After 2 days, transfected cells were selected with 450 µg/ml G418. Five days later, fresh medium without G418 was replaced. Ten days later, transfected cells were seeded into 96-well plates at the density of 1 cell/well by limiting dilution. Monoclonal cell lines were obtained after almost 20 days. Genomic DNA was extracted from cells and amplified using the primer set mentioned above. Sanger sequencing was performed to screen genomic mutation using the aforementioned forward primer. Sequencing primer for cDNA was 5′-TTTTCCCTACGTGGAATTGG-3′.

YAP overexpression transfection and siRNA transfection

SVG cells (4×10^5) were plated into 6 cm dishes in normal media. The next day, cells were transfected with pLEX-YAP or pLEX plasmid (Addgene) by using Lipofectamine 3000. After 2 days, transfected cells were harvested for cell counting and protein collection.

Non-silencing siRNA and ITGB4 siRNA targeting ITGB4-3541): 5′-GCUCAGCAACCCUAAGUUUTTAAA CUUAGGGUUGCUGAGCTT-3′ were purchased from abm (Richmond, BC, Canada). Cell transfection was performed using DNAfectin (abm) following the manufacture's instruction at a ratio of siRNA to reagent is 2 µg:7 µl. Cells were harvested 48 h after transfection for experiments.

2-HG measurement by gas chromatography/mass spectrometry (GC/MS)

Levels of 2-HG were measured using GC/MS analysis as follows: to 2 ml of media or cell lysate, 15 µg of 2-ketoglutarate-d6 was added and the samples acidified and extracted twice with 2 ml ethylacetate. The pooled solvent layers were evaporated under nitrogen and the residues derivatized with BSTFA + 1% TMCS. For SIM-GC/MS analysis, 1 µl was injected into an Agilent 6890/5973 GCMS system utilizing a Restek Rtx-1MS 30 m, 0.25 mm ID capillary column. The GC oven program was as follows: 70 °C for 2 min.; 4 °C/min ramp to 220 °C; 10 °C/min ramp to 290 °C; hold for 15 min. Mass spectrometric data were collected in the selected ion mode at $m/z = 247$ for native 2-HG and $m/z = 350$ for 2-ketoglutarate-d6. Calibration curves were constructed by mixing 15 µg of 2-ketoglutarate-d6 with 0.2–20 µg of 2-HG. Identification of D-2-HG was confirmed by mass spectral analysis in total ion current mode.

Quantitative real-time PCR

Total RNA was extracted using RNeasy Mini Kit (Qiagen, Mansfield, MA). After reverse transcription using MuLV reverse transcriptase (Applied Biosystems, Calsbad, CA) and Oligo(dT) primer, quantitative real-time PCR (qRT-PCR) was performed using SYBR Green PCR Mix (Applied Biosystems) and IQ5 detection system (Bio-Rad, Hercules, CA). Primer sequences used in this study were listed in Supplemental Table 5. Relative gene expression was normalized to 18 S rRNA or GAPDH.

Immunoblot and Immunocytochemistry

Total cellular protein was extracted with radio-immunoprecipitation assay buffer containing protease and

phosphatase inhibitors (Calbiochem, MA) and sonicated for 15 s; the suspensions were centrifuged at 3,000×*g* for 10 min. Protein concentration was determined by the Coomassie Protein Assay (Thermo Scientific). SDS-PAGE was performed with 30 μg total proteins using 4–12% gradient Tris-glycine gels (LI-COR Biosciences, Lincoln, NE). Western blot analysis was performed using the Quantitative Western Blot System, with secondary antibodies labeled by IRDye infrared dyes (LI-COR Biosciences). The antibodies used for this study were listed below; most of them from Cell signaling Inc (Danvers, MA) unless otherwise stated: IDH1 mutant-specific (R132H form): Dianova (Hamburg, Germany, DIA-H09); IDH1 (mAb #8137); TNC (Millipore); brevican (Abcam); YAP, cyclin A, E1 and CDKs, ERK and phospho-ERK, p38 and phospho-p38, JNK and phospho-JNK, Jagged 1, NICD1 and NOTCH1, β –catenin, AKT and phosphor-AKT, IKK β, STAT3 and β-actin (Sigma).

For staining, cells grown on chamber slides were fixed with 4% paraformaldehyde for 30 min at 4°C and permeabilized with PBS containing 0.1% Triton X-100 for 10 min. The cells were then incubated with primary antibodies at 4 °C overnight and then incubated with appropriate corresponding secondary antibodies for 1 h at room temperature. Slides were mounted with vectashield antifade solution containing 4′-6-Diamidino-2-phenylindole (DAPI, Vector Laboratories, Burlingame, CA) and observed under fluorescent microscopy. Immunofluorescent images were taken and analyzed using Axiovision software (Zeiss, Germany).

Histone extraction and detection of histone methylation

Histones were isolated with a histone extraction kit (ab113476; Abcam), following the manufacturer's procedure. Histone Protein (2 μg) was separated by 4–20% Tris-Glycine gels, and transferred to nitrocellulose membranes. Primary antibodies used for Western blotting are as follows: H3K4Me3, H3K9Me2, H3K9Me3, H3K27Me3, H3K36Me2, H3K36Me3, and H3K79Me3 (Cell Signaling biotechnology, 1:1000).

Cell migration assay

For migration assays in transwells (Corning, Lowell, MA), cells were suspended at 5×10^5 cells/ml; 100 μl of the cell suspension were added to the upper chamber of the transwells in serum-free medium [37]. Six hundred microliters of medium containing 10% FCS was added to the lower chamber. After 4–24 h incubation at 37 °C, cells were fixed with Diff-Quick kit (Thermo Fisher Scientific). Cells on the upper side of the transwells were gently wiped off with Q-tips. Cells migrating through the filter were stained with

DAPI. Migration was quantified by counting cells on five selected fields of view per transwell in at least three independent experiments [37, 38].

Cell Cycle Analysis

Cell cycle was analyzed by flow cytometry on a FACS-Calibur (Becton-Dickinson, Mountain View, CA) [39]. Briefly, SVG cells were synchronized by plating into 0.1% FCS medium for 36 h followed by stimulating with 10% FCS for indicated time points. To harvest, the cells were trypsinized and dissociated by pipetting, fixed with 75% ethanol at 4 °C for 30 min, then incubated with DNase-free RNase at 37 °C for 30 min, and propidium iodide (100 ng/ml) for 1 h at 37 °C. The percentage of cells at each cell-cycle phase (G1/G0, S, and G2/M) was analyzed using CellQuest software (Becton-Dickinson).

Global DNA methylation and gene expression analysis

The Infinium MethylationEPIC BeadChip (GEO platform accession number: GPL21145) was used to interrogate the methylation level of *IDH1* WT and *IDH1*[R132H/WT] clones. We analyzed DNA methylation data to identify differential methylated sites and regions Using RnBeads [40]. The promoter regions of the reference genes are defined as the regions across 1,500 bp upstream and 500 bp downstream of transcript start sites. Methylation site or region was defined as significantly changed if it has absolute differential methylation level >0.05 and FDR < 0.05.

RNAs from WT and two *IDH1*[R132H/WT] clones were subjected to Illumina HiSeq next generation sequencing following the standard amplification and library construction protocol provided by the Johns Hopkins Deep Sequencing and Microarray Core Facility [26]. Sequencing was performed using 100-base paired-end reads, with average 32 million reads generated from each sample. More than 66.7% of the sequencing reads were uniquely mapped to the human genome. Raw data were mapped to the hg19 genome assembly using STAR [41]. We then calculated the counts of reads for each gene through HTSeq [42]. DESeq was further used to identify the differentially expressed genes [43]. The gene was defined as significantly changed if it has absolute log2 fold change > 1 and FDR < 0.01.

We associated the gene expression with DNA methylation in its promoter regions. According to the differential gene expression (upregulated vs. downregulated) and the differential methylation (hyper-methylated vs. hypo-methylated), we overlapped differential genes into four categories.

All the raw data for our large-scale studies have been deposited in GSE103558 (for both DNA methylation and

RNA-seq data). We also obtained the subseries GSE103556 (for DNA methylation) and GSE103557 (for RNA-seq data).

Human glioma tissue collection

Patient-derived primary GBM tissues were obtained at the Johns Hopkins Hospital under the appropriate approval of the Institutional Review Board (IRB). All primary GBM cell lines were derived and established from excess tumor tissue from patients undergoing surgical resection for GBM. GBM cell line derivation and culture protocols were as previously described [44].

Intracranial tumor implantation

All animal protocols were approved by the Johns Hopkins School of Medicine Animal Care and Use Committee. Each 6–8 week old female BALB/c strain immunodeficient (SCID) mouse received 100,000 viable SVG cells in 2 μL PBS by stereotactic injection to the right caudate/putamen (AP = 0 mm, ML = −2.5 mm, and DV = −3.0 mm). After 6 months, mice were killed and perfused with 4% paraformaldehyde; the brains were removed for histological analysis.

Statistical analysis

Statistical analysis was performed using Prizm software (GraphPad, La Jolla, CA, www.graphpad.com). Post hoc tests included the Students T-test and Tukey multiple comparison tests as appropriate. Data are represented as mean value±standard error of mean (S.E.) unless otherwise stated. Significance was set at $P < 0.05$.

Compliance with ethical standards

Conflict of interest The authors declare that they have no conflict of interest.

References

1. Parsons DW, Jones S, Zhang XS, Lin JCH, Leary RJ, Angenendt P, et al. An integrated genomic analysis of human glioblastoma Multiforme. Science. 2008;321:1807–12.
2. Yan H, Parsons DW, Jin G, McLendon R, Rasheed BA, Yuan W, et al. IDH1 and IDH2 mutations in gliomas. N Engl J Med. 2009;360:765–73.
3. Hartmann C, Meyer J, Balss J, Capper D, Mueller W, Christians A, et al. Type and frequency of IDH1 and IDH2 mutations are related to astrocytic and oligodendroglial differentiation and age: a study of 1,010 diffuse gliomas. Acta Neuropathol. 2009;118:469–74.
4. Mardis ER, Ding L, Dooling DJ, Larson DE, McLellan MD, Chen K, et al. Recurring mutations found by sequencing an acute myeloid leukemia genome. N Engl J Med. 2009;361:1058–66.
5. Kang MR, Kim MS, Oh JE, Kim YR, Song SY, Seo SI, et al. Mutational analysis of IDH1 codon 132 in glioblastomas and other common cancers. Int J Cancer. 2009;125:353–5.
6. Louis DN, Perry A, Reifenberger G, von Deimling A, Figarella-Branger D, Cavenee WK, et al. The 2016 World Health Organization Classification of Tumors of the Central Nervous System: a summary. Acta Neuropathol. 2016;131:803–20.
7. Watanabe T, Nobusawa S, Kleihues P, Ohgaki H. IDH1 mutations are early events in the development of astrocytomas and oligodendrogliomas. Am J Pathol. 2009;174:1149–53.
8. Labussiere M, Idbaih A, Wang XW, Marie Y, Boisselier B, Falet C, et al. All the 1p19q codeleted gliomas are mutated on IDH1 or IDH2. Neurology. 2010;74:1886–90.
9. Piaskowski S, Bienkowski M, Stoczynska-Fidelus E, Stawski R, Sieruta M, Szybka M, et al. Glioma cells showing IDH1 mutation cannot be propagated in standard cell culture conditions. Br J Cancer. 2011;104:968–70.
10. Luchman HA, Stechishin OD, Dang NH, Blough MD, Chesnelong C, Kelly JJ, et al. An in vivo patient-derived model of endogenous IDH1-mutant glioma. Neuro Oncol. 2012;14:184–91.
11. Hsu PD, Lander ES, Zhang F. Development and applications of CRISPR-Cas9 for genome engineering. Cell. 2014;157:1262–78.
12. Richardson CD, Ray GJ, DeWitt MA, Curie GL, Corn JE. Enhancing homology-directed genome editing by catalytically active and inactive CRISPR-Cas9 using asymmetric donor DNA. Nat Biotechnol. 2016;34:339–44.
13. Komor AC, Kim YB, Packer MS, Zuris JA, Liu DR. Programmable editing of a target base in genomic DNA without double-stranded DNA cleavage. Nature. 2016;533:420–4.
14. Major EO, Miller AE, Mourrain P, Traub RG, de Widt E, Sever J. Establishment of a line of human fetal glial cells that supports JC virus multiplication. Proc Natl Acad Sci USA. 1985;82:1257–61.
15. Ferenczy MW, Johnson KR, Steinberg SM, Marshall LJ, Monaco MC, Beschloss AM, et al. Clonal immortalized human glial cell lines support varying levels of JC virus infection due to differences in cellular gene expression. J Neuroimmune Pharmacol. 2013;8:1303–19.
16. Bargonetti J, Reynisdottir I, Friedman PN, Prives C. Site-specific binding of wild-type p53 to cellular DNA is inhibited by SV40 T antigen and mutant p53. Genes Dev. 1992;6:1886–98.
17. Duncan CG, Barwick BG, Jin G, Rago C, Kapoor-Vazirani P, Powell DR, et al. A heterozygous IDH1R132H/WT mutation induces genome-wide alterations in DNA methylation. Genome Res. 2012;22:2339–55.
18. Turcan S, Rohle D, Goenka A, Walsh LA, Fang F, Yilmaz E, et al. IDH1 mutation is sufficient to establish the glioma hypermethylator phenotype. Nature. 2012;483:479–U137.
19. Flavahan WA, Drier Y, Liau BB, Gillespie SM, Venteicher AS, Stemmer-Rachamimov AO, et al. Insulator dysfunction and

oncogene activation in IDH mutant gliomas. Nature. 2016;529:110–4.

20. Gumbiner BM, Kim NG. The Hippo-YAP signaling pathway and contact inhibition of growth. J Cell Sci. 2014;127:709–17.

21. Licciardello MP, Mullner MK, Durnberger G, Kerzendorfer C, Boidol B, Trefzer C, et al. NOTCH1 activation in breast cancer confers sensitivity to inhibition of SUMOylation. Oncogene. 2015;34:3780–90.

22. Konsavage WM Jr., Kyler SL, Rennoll SA, Jin G, Yochum GS. Wnt/beta-catenin signaling regulates Yes-associated protein (YAP) gene expression in colorectal carcinoma cells. J Biol Chem. 2012;287:11730–9.

23. Verhaak RG, Hoadley KA, Purdom E, Wang V, Qi Y, Wilkerson MD, et al. Integrated genomic analysis identifies clinically relevant subtypes of glioblastoma characterized by abnormalities in PDGFRA, IDH1, EGFR, and NF1. Cancer Cell. 2010;17:98–110.

24. Ma S, Jiang B, Deng W, Gu ZK, Wu FZ, Li T, et al. D-2-hydroxyglutarate is essential for maintaining oncogenic property of mutant IDH-containing cancer cells but dispensable for cell growth. Oncotarget. 2015;6:8606–20.

25. Sulkowski PL, Corso CD, Robinson ND, Scanlon SE, Purshouse KR, Bai H, et al. 2-Hydroxyglutarate produced by neomorphic IDH mutations suppresses homologous recombination and induces PARP inhibitor sensitivity. Sci Transl Med. 2017; 9:eaal2463.

26. Wan J, Su Y, Song Q, Tung B, Oyinlade O, Liu S, et al. Methylated cis-regulatory elements mediate KLF4-dependent gene transactivation and cell migration. eLife. 2017;6:e20068.

27. Lynch MD, Smith AJ, De Gobbi M, Flenley M, Hughes JR, Vernimmen D, et al. An interspecies analysis reveals a key role for unmethylated CpG dinucleotides in vertebrate Polycomb complex recruitment. EMBO J. 2012;31:317–29.

28. Sasaki M, Knobbe CB, Itsumi M, Elia AJ, Harris IS, Chio IIC, et al. D-2-hydroxyglutarate produced by mutant IDH1 perturbs collagen maturation and basement membrane function. Gene Dev. 2012;26:2038–49.

29. Cui D, Ren J, Shi J, Feng L, Wang K, Zeng T, et al. R132H mutation in IDH1 gene reduces proliferation, cell survival and invasion of human glioma by downregulating Wnt/beta-catenin signaling. Int J Biochem Cell Biol. 2016;73:72–81.

30. Fu Y, Zheng Y, Li K, Huang R, Zheng S, An N, et al. Mutations in isocitrate dehydrogenase 2 accelerate glioma cell migration via matrix metalloproteinase-2 and 9. Biotechnol Lett. 2012;34:441–6.

31. Sabit H, Nakada M, Furuta T, Watanabe T, Hayashi Y, Sato H, et al. Characterizing invading glioma cells based on IDH1-R132H

32. Miroshnikova YA, Mouw JK, Barnes JM, Pickup MW, Lakins JN, Kim Y, et al. Tissue mechanics promote IDH1-dependent HIF1alpha-tenascin C feedback to regulate glioblastoma aggression. Nat Cell Biol. 2016;18:1336–45.

33. Shi J, Zuo H, Ni L, Xia L, Zhao L, Gong M, et al. An IDH1 mutation inhibits growth of glioma cells via GSH depletion and ROS generation. Neurol Sci. 2014;35:839–45.

34. Wang G, Sai K, Gong F, Yang Q, Chen F, Lin J. Mutation of isocitrate dehydrogenase 1 induces glioma cell proliferation via nuclear factor-kappaB activation in a hypoxia-inducible factor 1-alpha dependent manner. Mol Med Rep. 2014;9:1799–805.

35. Moroishi T, Hansen CG, Guan KL. The emerging roles of YAP and TAZ in cancer. Nat Rev Cancer. 2015;15:73–79.

36. Tschaharganeh DF, Chen X, Latzko P, Malz M, Gaida MM, Felix K, et al. Yes-associated protein up-regulates Jagged-1 and activates the Notch pathway in human hepatocellular carcinoma. Gastroenterology. 2013;144:1530–42. e1512.

37. Xia S, Lal B, Tung B, Wang S, Goodwin CR, Laterra J, et al. Tumor microenvironment tenascin-C promotes glioblastoma invasion and negatively regulates tumor proliferation. Neuro Oncol. 2016;18:507–517.

38. Goodwin CR, Lal B, Zhou X, Ho S, Xia S, Taeger A, et al. Cyr61 mediates hepatocyte growth factor-dependent tumor cell growth, migration, and Akt activation. Cancer Res. 2010;70:2932–41.

39. Reznik TE, Sang Y, Ma Y, Abounader R, Rosen EM, Xia S, et al. Transcription-dependent epidermal growth factor receptor activation by hepatocyte growth factor. Mol Cancer Res. 2008;6:139–50.

40. Assenov Y, Muller F, Lutsik P, Walter J, Lengauer T, Bock C. Comprehensive analysis of DNA methylation data with RnBeads. Nat Methods. 2014;11:1138–40.

41. Dobin A, Davis CA, Schlesinger F, Drenkow J, Zaleski C, Jha S, et al. STAR: ultrafast universal RNA-seq aligner. Bioinformatics. 2013;29:15–21.

42. Anders S, Pyl PT, Huber W. HTSeq–a Python framework to work with high-throughput sequencing data. Bioinformatics. 2015;31:166–9.

43. Anders S, Huber W. Differential expression analysis for sequence count data. Genome Biol. 2010;11:R106.

44. Shah SR, David JM, Tippens ND, Mohyeldin A, Martinez-Gutierrez JC, Ganaha S, et al. Brachyury-YAP Regulatory Axis Drives Stemness and Growth in Cancer. Cell Rep. 2017;21:495–507.